

Electropneumatic Oscillators Using Nonlinear Inflatables

Elias De Smet, Lorenzo Migliorini, Edoardo Milana, Paolo Milani, and Benjamin Gorissen*

Animals and robots employ central pattern generators, networks that invoke rhythmic patterns from constant inputs, to orchestrate limb movements during locomotion. Artificial central pattern generators (CPGs) can be either implemented in software or constructed in a physical domain. The former lacks embodiment, inhibiting direct interactions with the physical world. The latter is restricted by a complex translation of abstract functions to the physical domain, e.g., negative feedback, if-then behavior, etc. Here, self-oscillators, a rudimentary type of central pattern generators, that find ground in both the pneumatic and electrical domains are demonstrated. First, the hysteretic behavior of previously developed conical membranes is analyzed in deformation space. This state-space behavior is then transformed to the electrical domain by means of a stretchable strain sensor. Next, an analog comparator distinguishes between the two states and instructs a pneumatic solenoid valve to counteract the current state. As a result, a stable oscillation emerges, with a frequency that is dominated by the physical characteristic of the pneumatic circuit. As such, the proposed electro-pneumatic oscillator provides a promising platform for building complex CPGs that control interactive neuromorphic robots.

neuromorphic architecture, distributing computation over a network of nonlinear elements, called neurons, which can be found throughout the whole organism. Functionality and thus also computation is distributed and embedded in the physical body, which is captured by the broad concept of embodied intelligence.^[5] Mimicking this neural architecture, neuromorphic robots display complex functionality that originate from a strikingly simple design. A first example dates back to Grey Walter's 1950 tortoise robot^[6] that can autonomously navigate past obstacles, harnessing motor control mechanisms that mimic nature's neural pathways. More recently, neuromorphic robots^[7] have seen a revival, aiming at mimicking neurobiology using very large-scale integration circuits composed of electronic components.^[8] At their core are central pattern generators (CPGs), which are neural networks that produce rhythmic patterns of

neural activity without receiving rhythmic inputs (Figure 1A). In its most distilled form, CPGs consist of two essential elements: a hysteretic element that converts a generalized flow into a discrete state and a sensing element that transforms the state of the hysteretic element into a counteracting generalized effort, driving the system to continuously switch states.


An example of such a CPG in the electrical domain is the Schmitt trigger oscillator circuit (Figure 1B), which is often used in microcontrollers to generate clock signals. More complex, software-implemented CPGs have been used to coordinate the movements of joints to make, e.g., a salamander robot^[9] walk,

1. Introduction

Classical robots follow a von Neumann computer architecture,^[1] where a central processing unit instructs output devices based on information from a memory unit and from input devices. They thrive in an industrial setting and will probably continue to do so for decades to come. Although modern robotics is making large strides forward,^[2,3] it remains a challenge to design robots that perform as well as their biological counterparts in unstructured environments that require continuous and autonomous adaptation.^[4] Instead of a von Neumann architecture, biology follows a

E. De Smet, B. Gorissen
Department of Mechanical Engineering
KU Leuven
3001 Leuven, Belgium
E-mail: benjamin.gorissen@kuleuven.be

E. De Smet, B. Gorissen
Flanders Make
3001 Leuven, Belgium

 The ORCID identification number(s) for the author(s) of this article can be found under <https://doi.org/10.1002/aisy.202400695>.

© 2025 The Author(s). Advanced Intelligent Systems published by Wiley-VCH GmbH. This is an open access article under the terms of the Creative Commons Attribution License, which permits use, distribution and reproduction in any medium, provided the original work is properly cited.

DOI: 10.1002/aisy.202400695

L. Migliorini, P. Milani
Interdisciplinary Centre for Nanostructured Materials and Interfaces (CIMaIna)
Physics Department
University of Milan
20133 Milan, Italy

E. Milana
Department of Microsystems Engineering – IMTEK
University of Freiburg
79110 Freiburg, Germany

E. Milana
Cluster of Excellence livMatS @ FIT—Freiburg Center for Interactive Materials and Bioinspired Technologies
University of Freiburg
79110 Freiburg, Germany

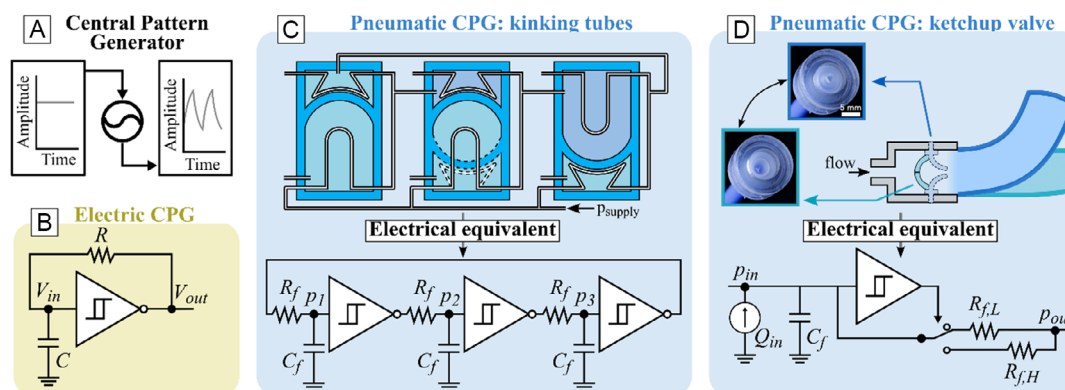


Figure 1. Artificial central pattern generators A) Schematic representation of a CPG, with a constant amplitude input and oscillating output. B) Schmitt trigger oscillator circuit. C) Self-oscillating ring of soft bistable valves with kinking tubes^[11] and equivalent electrical circuit. D) Pneumatic self-oscillating ketchup bottle valve^[14] with the equivalent electrical circuit.

by turning sensor readouts into motor commands. To make such robots sensitive to environmental influences, other sensor modalities can be incorporated to alter the CPG's function to humidity, temperature, etc. In contrast, biological neuromorphic systems achieve complex functionality without active centralized control, where external stimuli affect the operation of CPG's through, e.g., a change of body chemistry. Artificial systems with neuromorphic control architectures that swiftly adapt to environmental changes should therefore embody CPGs whose behavior is directly influenced by external mechanical, thermal, and/or chemical stimuli.

Examples of CPGs that are entirely situated in the mechanical domain can be found in the field of inflatable soft robotics, where the intricate characteristics of inflatable elements can be harnessed toward embodied intelligence.^[10] Rothmund et al. created a ring configuration of pneumatic bistable valves that give rise to spontaneous oscillations from a constant input (Figure 1C).^[11] This system is analog to an electrical circuit as shown in Figure 1C bottom (pressure \equiv voltage and mass flow \equiv current), where the bistable valves are represented by Schmitt triggers. Such pneumatic ring oscillators have been used as a CPG in the coordination of the limbs of a turtle-inspired soft robot^[12] and an aquarium cleaning robot.^[13] In a different philosophy, Van Laake et al.^[14] created oscillatory behavior using a single, ketchup valve inspired component (Figure 1D). Its equivalent electrical circuit is displayed in Figure 1D bottom where the ketchup valve is represented by an inverting Schmitt trigger with state-dependent variable resistance, behaving similarly to a Pearson-Anson oscillator.^[15] By combining multiple of these burst-through valves, a spontaneous synchronization emerges, which is used to drive four limbs of a crawling soft robot. In comparison to the aforementioned electrical or software-implemented CPGs, pneumatic oscillators benefit from a direct coupling between the generated pattern and the imposed structural deformations, as they are both depend on the inflation of the same structure. Environmental interactions, which occur in deformation space that superimpose deformation on the system, can directly influence the timing of actuation, resulting in global behavioral change. Drotman et al.^[12] used this direct coupling to change the locomotion direction of a walking robot when

bumping into a wall, without any software control. However, in comparison to the electrical domain, the creation of a sensing element that captures the discrete state of the hysteretic element using only fluidics is an uphill task.^[16,17]

Here we combine the advantages of both domains and create electropneumatic oscillators that incorporate hysteretic elements in the pneumatic domain with sensing elements in the electrical domain, where stretchable strain sensors form a link between both domains. As such, we aspire to offload some of the architectural complexity in the fluidic domain to the electrical domain, where the combination of a strain sensor and an electrical comparator is used as a sensing element while retaining 1) a direct coupling in deformation space and 2) time scales that are useful for locomotion purposes. With this research, we take a first step down a new avenue of hybrid electro-pneumatic robotics that mimic biological neuromorphic systems.

2. Results

2.1. Hysteretic Element

In its most distilled form, a central pattern generator incorporates a sensing element that instigates a counteraction to change the current state of a hysteretic element. Here we choose to implement hysteresis in the pneumatic domain, employing inflatables that express hysteretic behavior in their PV characteristic. Particularly interesting are membranes that have nonzero Gaussian curvature,^[18,19] as they exhibit rich nonlinear characteristics that even include isobaric (limit points in pressure) and isochoric snapping (limit points in volume), which are indicative of path dependent behavior, and thus hysteresis.^[18,20] In this study, we use truncated conical membranes^[21] (see **Figure 2A**), with radius r_0 of 30 mm, cone angle θ of 47°, and thickness t_m of 3.9 mm as indicated in Figure 2C. (for full dimension, we refer to Section S2, Supporting Information). We simulate their PV relationship using the finite element method (ABAQUS 2023/Standard), discretizing the geometry with 8-node linear brick solid elements, and employing an incompressible first order Ogden material model with material parameters $\mu = 340$ kPa and $\alpha = 4.75$ (material parameters are tuned based

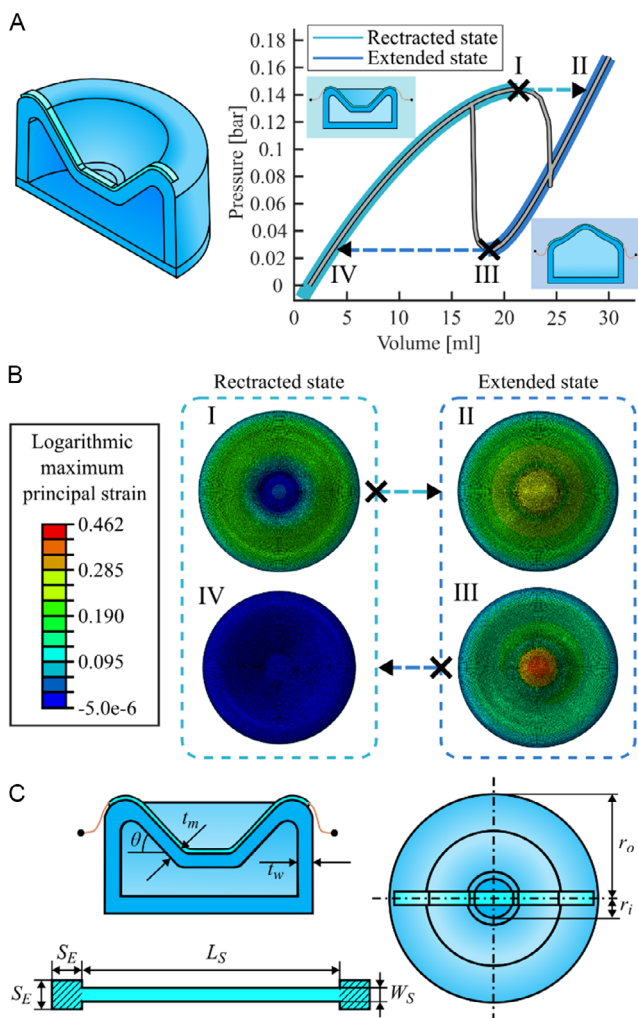


Figure 2. Soft pneumatic hysteretic element and soft electrical sensing element. A) 3D cross-cut illustration of the hysteretic element (left) with simulated pressure–volume (PV) graph using finite element modeling (right), with marked retracted (light blue) and extended (dark blue) deformation states and corresponding deformation in inset pictures. When inflating/deflating using pressure loading, the element transitions from unstable (I,III) to stable (II,IV) limit points. B) Top view of finite element simulated deformations at instances I–IV, showing logarithmic maximum principle strain. Marked on the figure are the retracted and extended states and the occurring transitions, corresponding to the subfigure above. C) Cross-cut and top view illustration of the hysteretic element with adhered sensing element.

on experimental data). We pressurize the membranes by supplying incompressible fluid under volume control to the internal cavity and simulate the PV curve via a dynamic implicit method, using the discretized Newton–Raphson (Full-Newton) algorithm.^[22] The simulated PV characteristic, as shown in Figure 2A, displays intricate nonfunctional behavior, with two limit points in pressure (I for inflation and III for deflation), confining a large hysteretic zone. This simulated characteristic allows us to predict the behavior when loading with a pressure input: during inflation, and thus when increasing the pressure inside the cavity, the membrane gradually deforms until point I.

Inflating the structure further triggers a mechanical instability where the membrane rapidly everts, transitioning to a stable deformation state in point II at an equal pressure but increased volume compared to point I. Following this transition, the conical membrane remains everted, almost linearly increasing its volume when increasing the internal pressure. This deformation state is defined as the extended state and is marked by the dark blue line in Figure 2A. During a subsequent deflation, the membrane will remain in the extended state until the pressure decreases below the lower pressure threshold in point III. At this point, deflation triggers again an instability, with the membrane snapping back to the retracted state (light blue line in Figure 2A), until reaching the stable configuration at point IV, with the same pressure as point III, but lower volume. At a pressure between upper and lower snapping thresholds, the membrane is bistable, having two stable states: extended or retracted. Within this pressure region, the state depends not only on the cavity pressure but also on the pressure history, and thus exhibits hysteresis.

2.2. Sensing Element

To sense the state of the nonlinear inflatable membrane, we are interested in global characteristics that have a different value in both states. Rothmund et al.^[11] used the apex height of conical membranes to pinch off a tube, as this height shows low variability within both states (snapped or not snapped), but greatly differs between states. Here we make use of the strain profile on the top side of the membrane (as is shown in Figure 2B), which manifests a similar effect. In the retracted state (state IV to I), it can be seen that the top side of the membrane experiences on average low strains (blue to green colored max principle strains). However, in the extended state (state II to III), the same section experiences higher average strains (green to yellow/orange colored max principle strains). Here, we capture these average strains by adhering a soft strain sensor to the top side of the actuator, indicated in light blue in Figure 2A,C. The employed strain sensor constitutes a thin rubber film with Au nanoparticles partially implanted underneath its surface, with the manufacturing process and characterization detailed in ref. [23], showing a reversible change of electrical properties when applying mechanical strain and a high gauge factor ($GF = \frac{\Delta R/R}{\Delta L/L}$) of about 65. By using a soft silicon rubber as the thin rubber film (Ecoflex 00-30, Smooth-On, inc.), we minimize the influence the strain sensor has on the functioning and characteristics of the hysteretic element. The strain-sensitive region of the sensor (70×4 mm) is centered and attached using liquid Ecoflex 00-30 rubber on top of the pneumatic actuator, molded from Dragonskin 30 (Smooth-On, inc) where for the fabrication process we refer the reader to Section S1, Supporting Information. The electrical connection is made by means of square protrusions (8×8 mm) on either end of the strain sensor that incorporate electrical wires.

Figure 3A shows snapshots of the fabricated hysteretic element (for which the fabrication process is elaborated in Section S2, Supporting Information) with adhered electrical sensing element both in the extended (dark blue) and retracted state (light blue). Its behavior is experimentally verified by performing a volume-controlled PV-inflation test, where we inflate

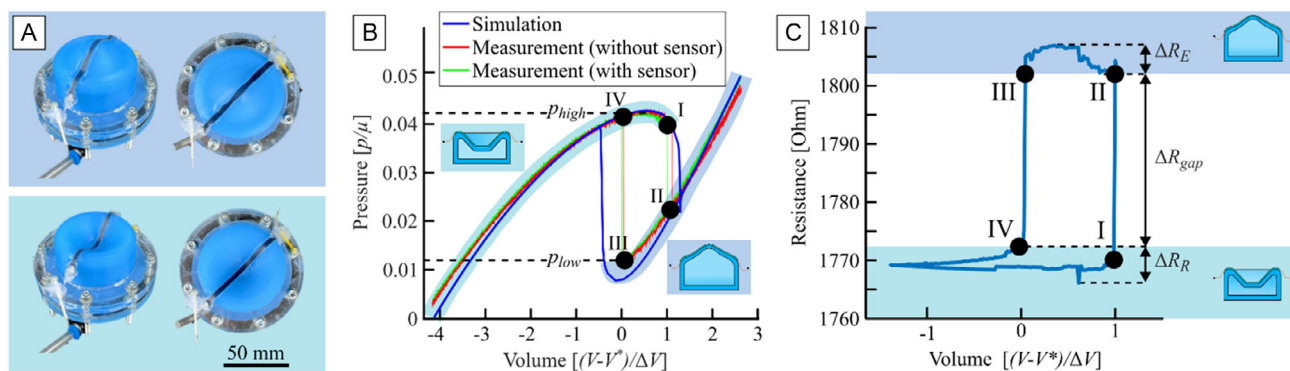


Figure 3. Experimental results of hysteretic element with adhered sensing element. A) Prototype with bistable pneumatic actuator as the hysteretic element (blue) and adhered strain sensor as the sensing element (black) in the extended (top) and retracted (bottom) state. Scale bar indicates 50 mm. B) Dimensionless pressure–volume (PV) curve, comparing FEM simulated against measured data. Marked retracted (light blue) and extended (dark blue) deformation states and corresponding deformation depiction, as well as high and low limit pressure levels. Pressure is nondimensionalized by scaling with modeled shear modulus μ . Volume nondimensionalized by centering with V^* (measured volume at extended state lower limit) and scaling by ΔV (measured volume enclosed by hysteresis loop). C) Measured strain sensor resistance (blue line) as a function of dimensionless volume. The extended/retracted states are marked with corresponding dark/light blue bar, with a corresponding depiction of the deformation. Black dots mark time instances I–IV, corresponding to those in subfigure B.

the truncated conical membrane with water using a syringe drive, simultaneously registering the internal pressure and the electrical resistance of the strain sensor (see Section S3, Supporting Information for details, and Video S1, Supporting Information for a close-up of the actuated membrane with strain sensor attached). In Figure 3B, we compare the numerical (blue line) and experimental (red line) PV characteristics of a bare conical membrane (without strain sensor), with inset images displaying snapshots of the numerical deformations. We found good agreement between simulations and experiments, showing limit points both in pressure and in volume, near the numerically predicted limit points. It is apparent that stability is lost earlier in experiments, which can be attributed to unavoidable imperfections during fabrication, reminiscent of the knockdown factor of spherical shells.^[24] When repeating the same test for a conical membrane with an adhered sensor (green line), we see negligible influence of the sensor on the PV characteristics, where most importantly, limit points in pressure/volume remain unaltered, which is a result of the order of magnitude of difference between the shear modulus of the membrane material and sensor material (Dragonskin 30 vs. Ecoflex 00-30).^[25] Here we nondimensionalize volume by centering with V^* (measured volume at the extended state lower limit, marked by time instance III) and scaling by ΔV (measured volume enclosed by hysteresis loop). By definition, the hysteresis loop spans a dimensionless volume from 0 to 1. In Figure 3C, we display the resistance (blue line) that is measured in the strain sensor as a function of dimensionless volume. In the unloaded state, a resistance of about 1768Ω is measured that only varies slightly while increasing the internal volume. At time instance I, a dimensionless volume of 1 is reached and the continuous inflation results in a rapid inversion of the membrane to the second, extended, state, with a coinciding jump of resistance to reach 1805Ω . Further inflation and initial deflation do not result in drastic changes of this resistance value. However, at time instance III, when deflation reaches another limit point at a dimensionless volume of 0,

the membrane resets to its initial, retracted, state, with a resistance value that again approximates the starting resistance value, before the loading cycle. The resistance shows a low variability within each state, where the resistance in the extended state (ΔR_E) only varies with 6Ω (between 1766 and 1772Ω), while in the retracted state, the resistance varies with 5Ω (ΔR_R , between 1803 and 1808Ω). Further, there is a large difference in resistance value between both states, with minimal separating resistance (ΔR_{gap}) being 31Ω . To verify the stability of the sensor, we subsequently conducted 90 inflation tests, while capturing the strain sensor. Over these 90 inflation cycles, ΔR_R had an average value of 6.23Ω , varying by $\pm 3.81 \Omega$, ΔR_E had an average value of 5.09Ω , varying by $\pm 0.68 \Omega$, and ΔR_{gap} had an average value of 28.40Ω , varying by $\pm 2.39 \Omega$. Additional tests with increased influx rates showed negligible change of these differential values (see Section S4, Supporting Information); however, it should be noted that we saw some drift of the absolute resistance values with increased number of actuation cycles, which is indicative of global effects, e.g., heating (see Section S5, Supporting Information). In general, the sensor is suitable to differentiate the states of the inflatable actuator, as it shows low variability of resistance within a certain state, while registering a big change in resistance when changing states.

2.3. Electropneumatic Oscillator

Thus far we have shown that a conical membrane with an adhered strain sensor has all necessary conditions to induce oscillatory behavior. The simplicity of a hysteretic electropneumatic element consists of the ease with which the full oscillatory network can be created. In its most rudimentary form, the output of an electric comparator, which senses if the resistance of the sensor is above or below 1790Ω , can be used to control the pressure input to the membrane. When sensing a higher resistance, and thus an extended state, the membrane needs to be deflated. When sensing a lower resistance, the membrane needs to be

inflated. This event-based control strategy is implemented using an analog electronic circuit, which instructs a solenoid valve to connect to a high pressure (p_{high} , above the forward limit pressure of the membrane—see pressure at point I, Figure 2) leading to inflation, or to a low pressure (p_{low} , below the backward limit pressure—see pressure at point III, Figure 2). As such, an electropneumatic oscillator system (see Figure 4A) is developed, transitioning from the pneumatic to the electrical domain using our hysteric membrane, and from the electrical to pneumatic domain using a solenoid valve. When implementing this circuit in reality (see Section S6, Supporting Information for details), setting $p_{\text{high}} = 15 \text{ kPa}$ and $p_{\text{low}} = 0 \text{ kPa}$, we see a cyclically varying pressure inside the conical membrane, as shown in Figure 4B. The pressure varies between 14.5 and 4.2 kPa, being the forward and backward limit pressure of the membrane, with a stable period of 8.23 s. Figure 4C shows snapshots of the oscillating membrane at four equidistant instances during a single oscillation period, as marked in Figure 4B.

As this system has roots in the electrical and pneumatic domains, expansion to more complex architectures can occur in both. Here we show this by adding a pneumatic cylinder to

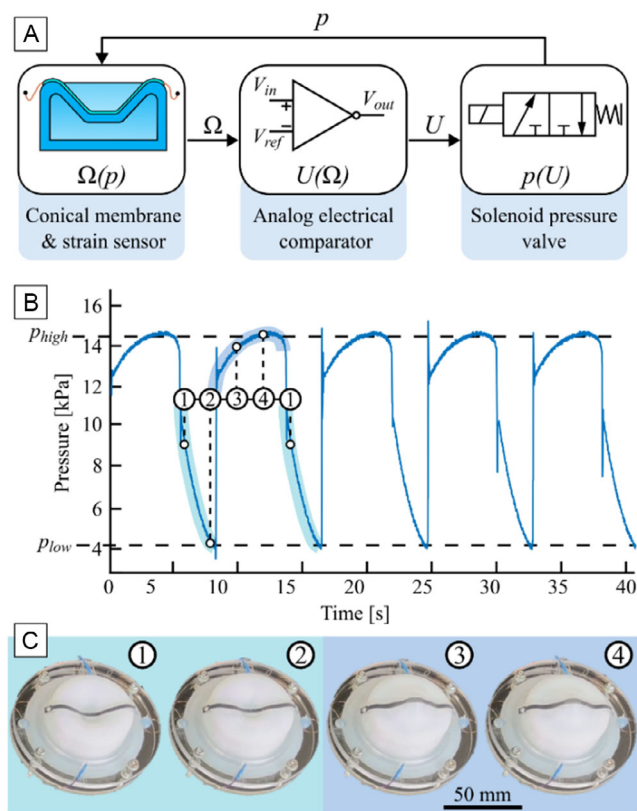


Figure 4. Electropneumatic oscillator. A) Schematic representation featuring a closed-loop system with three transfer functions. B) Measured pressure inside the conical membrane as a function of time during five oscillation periods. The two pressure limits (p_{high} and p_{low}) are indicated by dashed lines, numbered markers indicate four equally spaced time instances during a single oscillation period, with accompanying pressure levels indicated by white dots. C) Snapshots of the oscillating conical membrane at the time instances marked in subfigure B.

the system that we want to synchronize with the snapping of the conical membrane. Adding a parallel pneumatic branch, consisting of a tube and pneumatic cylinder, to the current solenoid valve would add a parasitic capacitance to the system, increasing the global system's time constant and thus decreasing the oscillation frequency. Alternatively, a parallel connection can be made in the electrical domain (Figure 5A,B), adding a second dedicated solenoid valve for controlling the pneumatic cylinder, where the controlling signal for this solenoid valve follows the original electrical signal. The original pneumatic circuit thus acts a master circuit that controls all timing aspects, instructing the new slave circuit when to actuate. As there is no bidirectional coupling between both circuits, the master circuit does not “see” the parasitic dynamics of the slave circuits, resulting in oscillations at an unchanged frequency. Figure 5C shows snapshots of the master circuit's oscillating membrane and the accompanying slave pneumatic cylinder at equally spaced time instances during a single oscillation period, as indicated in Figure 5D as well. It can be observed that the spring-loaded pneumatic cylinder retracts and extends synchronously with the conical membrane.

The dynamic behavior of the oscillator is dominated by the pneumatic domain, as it takes time to inflate the membrane through a narrow tube. The oscillation speed is thus governed by physical quantities, and not by an abstract parameter value stored in software. This direct coupling enables to influence the system dynamics by manipulating the underlying physical components,^[19] creating a direct avenue for environmental sensing.^[26] For our oscillator, the dynamics of the pneumatic subsystem can be understood by modeling it as a first-order system with time constant $\tau = R_f C_p$. C_p is the pneumatic capacitance, which can be thought of as the volume in the circuit where energy can be stored by compression of the gas, and R_f (see Figure 5A) is the combined fluidic resistance of the tubing in the pneumatic circuit, which can be approximated by the Darcy-Weisbach equation: $R_f = \frac{128}{\pi} \mu \frac{L}{D^3}$, with μ the dynamic viscosity of air, and L and D the length and diameter of the tubing. Here we display the ease at which the oscillation frequency can be adapted by varying physical parameters of the pneumatic circuit. In Figure 5D, we plot in function of the fluidic resistance R_f , which was changed by introducing needles with different diameters and lengths in the fluidic circuit, the average measured oscillation period T_{avg} (data points are also tabulated in Section S7 and Video S2, Supporting Information shows experiments of three data points). First, we see that a change in fluidic resistance of 4 orders in magnitude (3.16×10^{-3} – $1.84 \text{ GPa s m}^{-3}$) gives rise to an average oscillation period that also changes with 4 orders of magnitude (0.67–157 s). Second, we confirm the linear relationship between oscillation frequency and resistance, meaning that the system can be accurately modeled as an RC circuit (see Section S7, Supporting Information for details and statistical analysis of the data). We conclude that the oscillation frequency remains constant in time when geometrical parameters are kept constant, whereas changing these geometrical parameters, or altering them during operation (e.g., pinching of a tube to reduce the cross section), has a large influence on the oscillation frequency. However, the shape of the oscillations in steady state remains unaffected. This can be observed from Figure 5E, showing pressure oscillations for four different fluidic

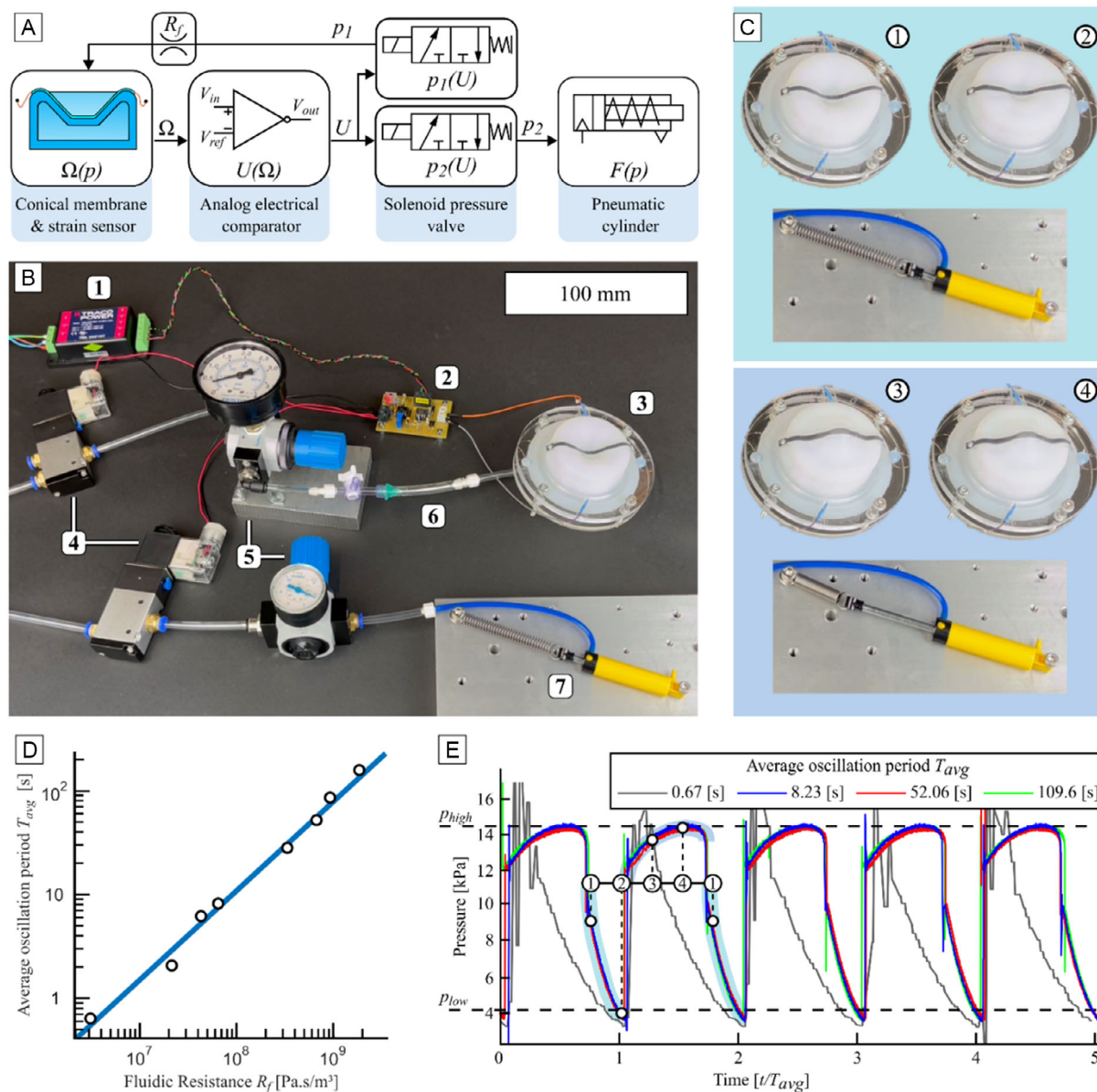


Figure 5. Master electropneumatic circuit with slave pneumatic cylinder. A) Schematic representation of the closed-loop master system and accompanying slave system. A fluidic resistance R_f is present on the pressure supply of the conical membrane. B) Experimental electropneumatic system (1. Power supply, 2. Analog electrical comparator, 3. Conical membrane with strain sensor, 4. Solenoid valves, 5. Pressure regulators, 6. Fluidic resistance and 7. Pneumatic cylinder). C) Snapshots of the oscillating conical membrane at time instances marked in subfigure E and accompanying pneumatic cylinder actuation. D) Average measured oscillation period T_{avg} in relation to calculated fluidic resistance R_f on a double logarithmic scale, with linear fitted curve (blue). E) Pressure oscillations for four fluidic resistances as a function of time, nondimensionalized by scaling with their respective average measured oscillation period T_{avg} . Two pressure limits (p_{high} and p_{low}) indicated with dashed lines. Four equally spaced time instances over a single oscillation period marked with corresponding pressure levels.

resistances as a function of time, nondimensionalized by scaling with the respective average period T_{avg} of the oscillations. Regardless of their original timescale, all time normalized oscillations coincide well with each other, except for the fastest oscillations with a period of 0.67 s, where vibrations excited by snapping transitions have not fully died out yet, resulting in the dissimilar pressure measurement over time. This effect can also be seen on Video S2, Supporting Information.

3. Discussion and Conclusion

In summary, we have introduced a novel central pattern architecture that harnesses the physical characteristics of truncated conical membranes in combination with an analog electrical comparator to create robust oscillations. This behavior originates from the membrane's hysteretic pressure–volume relationship that exhibits two distinct states: retracted and extended. This

unique behavior is captured using an electrical strain sensor, showing discrete resistance values in both states, enabling to use this signal to instigate state-dependent behavioral actions in the electrical domain. By feeding the electrical signal into a solenoid valve, we close the negative feedback loop, giving rise to stable oscillations. Previously, Rothmund et al. demonstrated that fixed frequency oscillations emanate from a ring configuration of buckling shell valves, while Van Laake et al. showed that fluidic hysteretic valves automatically phase lock because of a negative coupling through the actuation fluid, which resembles mutual inhibition typical to CPG systems.^[11,14] Compared to CPGs reported solely in the electrical^[7] or fluidic domain,^[12] the low-complexity architecture proposed here couples both domains, resulting in a modular platform suited for tuning CPG characteristics while offering a toolbox to benefit from environmental interactions. In our current implementation of an oscillator, the two phases (inflation and deflation) have very similar dynamic behaviors, as the fluid flow is restricted in both phases by the same fluidic resistance, and the oscillation frequency is not controlled, but rather imposed by a fixed diameter and length of an unchanged flow restrictor. Building on these results, further investigation can go to the control of phase difference within a single cycle, by incorporating variable flow restrictors where the orifice can be continuously tuned by means of a pressure or an electrical voltage, for which various commercial solutions exist, or even by means of external influences like magnetic fields^[27] or temperature,^[28] having parallels with neuromodulation. Additionally, the coupling to the electrical domain can be further explored, for example, by designing a system where the snapping of one membrane would restrict the flow to a second parallelly loaded membrane, emulating mutual inhibition. This would require extending our system to incorporate multiple nodes (conical membranes with strain sensors), which could prove a strategy to efficiently control and orchestrate multiple degrees of freedom. For instance in a robotic system, two nodes can be implemented per limb to control a local stepping motion, where an overarching pattern generator orchestrates the global coordination between legs to achieve for instance a trotting gate. Environmental interactions could then be perceived by the physical components that make up the CPG, directly influencing the global behavior of the mobile robot. For example, external forces stemming from environmental interactions could pinch a flexible tube causing it to act as a variable flow resistance, or could load a bistable shell thus altering its pressure–volume characteristics. However, further studies are required to minimize the size and weight to better accommodate the robotic application.

Supporting Information

Supporting Information is available from the Wiley Online Library or from the author.

Acknowledgements

This research was supported by the Fund for Scientific Research-Flanders (FWO—G094920N) and the European Research Council (ERC starting grant ILUMIS—101076036). Project within the MUSA—Multilayered Urban Sustainability Action—project, funded by the European Union—

NextGenerationEU, under the National Recovery and Resilience Plan (NRRP) Mission 4 Component 2 Investment Line 1.5: Strengthening of research structures and creation of R&D “innovation ecosystems”, set up of territorial leaders in R&D. E.M. acknowledges additional funding by the Deutsche Forschungsgemeinschaft (DFG, German Research Foundation) under Germany’s Excellence Strategy-EXC-2193/1-390951807.

Conflict of Interest

The authors declare no conflict of interest.

Author Contributions

Elias De Smet: conceptualization (lead); formal analysis (equal); investigation (equal); methodology (lead); validation (lead); visualization (lead); and writing—original draft (lead). **Lorenzo Migliorini:** conceptualization (supporting); formal analysis (equal); investigation (equal); methodology (supporting); validation (supporting); and writing—original draft (supporting). **Edoardo Milana:** conceptualization (supporting); formal analysis (supporting); methodology (supporting); and writing—review and editing (supporting). **Paolo Milani:** funding acquisition (supporting); resources (supporting); supervision (equal); and writing—review and editing (supporting). **Benjamin Gorissen:** conceptualization (supporting); funding acquisition (lead); methodology (supporting); resources (lead); supervision (equal); visualization (supporting); and writing—original draft (supporting). **Elias De Smet** and **Lorenzo Migliorini** contributed equally to this work.

Data Availability Statement

The data that support the findings of this study are available from the corresponding author upon reasonable request.

Keywords

central pattern generators, neuromorphic robots, oscillators, soft robotics

Received: August 12, 2024

Revised: November 29, 2024

Published online:

- [1] J. von Neumann, *IEEE Ann. Hist. Comput.* **1993**, *15*, 27.
- [2] C. Bartolozzi, G. Indiveri, E. Donati, *Nat. Commun.* **2022**, *13*, 1024.
- [3] J. Lee, J. Hwangbo, L. Wellhausen, V. Koltun, M. Hutter, *Sci. Rob.* **2020**, *5*, eabc5986.
- [4] T. Miki, J. Lee, J. Hwangbo, L. Wellhausen, V. Koltun, M. Hutter, *Sci. Rob.* **2022**, *7*, eabk2822.
- [5] J. B. R. Pfeifer, *How the Body Shapes the Way We Think: A New View of Intelligence*, MIT Press, Cambridge, MA, USA **2006**.
- [6] W. G. Walter, *Sci. Am. Mag.* **1950**, *182*, 42.
- [7] C. Mead, *NASA STI/Recon Tech. Rep. A* **1989**, *90*, 16574.
- [8] Y. Yang, C. Bartolozzi, H. H. Zhang, R. A. Nawrocki, *Eng. Appl. Artif. Intell.* **2023**, *126*, 106838.
- [9] A. J. Ijspeert, A. Crespi, D. Ryczko, J.-M. Cabelguen, *Science* **2007**, *315*, 1416.
- [10] B. Gorissen, E. Milana, A. Baeyens, E. Broeders, J. Christiaens, K. Collin, D. Reynaerts, M. De Volder, *Adv. Mater.* **2019**, *31*, 1804598.
- [11] P. Rothmund, A. Ainla, L. Belding, D. J. Preston, S. Kurihara, Z. Suo, G. M. Whitesides, *Sci. Rob.* **2018**, *3*, eaar7986.

- [12] D. Drotman, S. Jadhav, D. Sharp, C. Chan, M. T. Tolley, *Sci. Rob.* **2021**, 6, eaay2627.
- [13] W.-K. Lee, D. J. Preston, M. P. Nemitz, A. Nagarkar, A. K. MacKeith, B. Gorissen, N. Vasios, V. Sanchez, K. Bertoldi, L. Mahadevan, G. M. Whitesides, *Sci. Rob.* **2022**, 7, eabg5812.
- [14] L. C. van Laake, J. de Vries, S. Malek Kani, J. T. B. Overvelde, *Matter* **2022**, 5, 2898.
- [15] S. O. Pearson, H. S. G. Anson, *Proc. Phys. Soc. London* **1921**, 34, 204.
- [16] S. Wang, L. He, P. Maiolino, *IEEE Rob. Autom. Lett.* **2022**, 7, 112.
- [17] C. J. Decker, H. J. Jiang, M. P. Nemitz, S. E. Root, A. Rajappan, J. T. Alvarez, J. Tracz, L. Wille, D. J. Preston, G. M. Whitesides, *Proc. Natl. Acad. Sci.* **2022**, 119, e2205922119.
- [18] B. Gorissen, D. Melancon, N. Vasios, M. Torbati, K. Bertoldi, *Sci. Rob.* **2020**, 5, eabb1967.
- [19] N. Vasios, B. Deng, B. Gorissen, K. Bertoldi, *Nat. Commun.* **2021**, 12, 695.
- [20] C. Qiao, L. Liu, D. Pasini, *Adv. Sci.* **2021**, 8, 2100445.
- [21] B. Van Raemdonck, E. Milana, M. De Volder, D. Reynaerts, B. Gorissen, *Adv. Mater.* **2023**, 35, 2301487.
- [22] M. A. Crisfield, *Comput. Struct.* **1981**, 13, 55.
- [23] L. Migliorini, T. Santaniello, A. Falqui, P. Milani, *ACS Appl. Nano Mater.* **2023**, 6, 8999.
- [24] H. N. R. Wagner, C. Hühne, S. Niemann, *Int. J. Mech. Sci.* **2018**, 141, 58.
- [25] L. Marechal, P. Baland, L. Lindenroth, F. Petrou, C. Kontovounisios, F. Bello, *Soft Rob.* **2021**, 8, 284.
- [26] S. Zou, S. Picella, J. de Vries, V. G. Kortman, A. Sakes, J. T. B. Overvelde, *Nat. Commun.* **2024**, 15, 539.
- [27] P. Dunne, T. Adachi, A. A. Dev, A. Sorrenti, L. Giacchetti, A. Bonnin, C. Bourdon, P. H. Mangin, J. M. D. Coey, B. Doudin, T. M. Hermans, *Nature* **2020**, 581, 58.
- [28] V. Bazargan, B. Stoeber, *J. Microelectromech. Syst.* **2010**, 19, 1079.